Research Article ISSN Online: 2783-4859 Computational Mathematics and Computer Modeling with Applications

Received 26 February 2025
Accepted 6 October 2025

DOI: 10.48308/CMCMA.4.2.22
AMS Subject Classification: 92C40; 92D30; 65L10

Unveiling the significance of control factors on the vaccinated population for COVID-19 using the homotopy perturbation method

Aderonke Ola Oluwarotimi[a] **and Amos Oladele Popoola**[a]

The global emergence of the Coronavirus (Covid-19) has resulted in far-reaching implications, encompassing substantial loss of human lives and the revelation of vulnerabilities in health systems across the globe. In response to this crisis, we revisited a prior model and extended it by incorporating a vaccination control element. This novel addition involves introducing a control factor into the vaccinated class to examine the repercussions of frequent vaccine administration as a strategic measure to mitigate the spread of COVID-19. Of particular interest in our investigation is the exploration of the criteria for the existence of numerical solutions to the model, achieved through the application of the Homotopy Perturbation Method. Our preliminary findings demonstrate that the vaccine control factor exerts substantial effects on both the susceptible and recovery classes within the model. This research contributes to the understanding of the dynamics of COVID-19 transmission, providing insights that can inform public health strategies in the ongoing global battle against the pandemic.

Keywords: Covid-19; Vaccine control factor; Homotopy perturbation method.

1. Introduction

The emergence of Coronavirus (COVID-19) has had widespread consequences, leading to significant loss of life and exposing vulnerabilities in global health systems [14]. This unprecedented crisis necessitates innovative research to better understand and address the dynamics of COVID-19 transmission. A critical milestone in the fight against the pandemic was the introduction of the first COVID-19 vaccine on July 22, 2020 [14]. As vaccination efforts continue, it is essential to investigate their impacts on disease transmission and public health outcomes.

Mathematical modeling has become an indispensable tool in epidemiology, providing critical insights into the spread and control of infectious diseases. Traditional approaches often rely on ordinary or partial differential equations (ODEs/PDEs) to simulate transmission dynamics, as demonstrated by studies on disease-free equilibrium, stability analysis, and intervention strategies [6, 7, 19, 4, 31]. For instance, Koo et al. [19] modeled COVID-19 interventions in Singapore, highlighting the need for rapid responses to curb community transmission. Similarly, Ahmed et al. [4] emphasized the role of asymptomatic carriers in disease persistence, while ODE-based frameworks by Popoola et al. [28, 29], Oreyeni et al. [25], and Shah et al. [30] have been pivotal in modeling physical and biological systems. These methodologies, however, often overlook memory effects and hereditary traits inherent in real-world processes. To address these limitations, recent advances in modelling have revolutionized epidemiological modeling by capturing long-range dependencies and adaptive dynamics via fractional calculus. Fractional-order models now offer nuanced perspectives on disease control, from COVID-19 vaccination efficacy [22, 33] to malaria eradication strategies [10, 32]. For tuberculosis, Caputo fractional derivatives have refined predictions of treatment outcomes [23], while cholera models now incorporate environmental interactions more realistically [3]. This shift from integer-order to fractional-order systems has not only enhanced epidemiological accuracy but also extended to other domains.

Beyond public health, fractional calculus has proven transformative in financial systems, where it models adaptive behaviors like investment decision-making under uncertainty [24]. These interdisciplinary applications underscore the versatility of fractional-order frameworks in capturing complex, memory-dependent dynamics across both biological and socioeconomic systems. By

[a] *Department of Mathematical Sciences, Osun State University, Osogbo, Nigeria.*
[*] *Correspondence to: A.O. Oluwarotimi. Email: aderonke.oluwarotimi1@gmail.com*

bridging gaps between theoretical models and real-world phenomena, such approaches empower policymakers to design more resilient, data-driven interventions.

Before simulation, solving mathematical models is essential for investigating the influence of various parameters. However, obtaining analytical solutions can be challenging. Consequently, researchers often resort to numerical techniques, such as the homotopy perturbation method, to facilitate their analyses [15, 16, 8, 7]. For instance, Kolawole et al. [18] utilized this method to analyze the impacts of vaccination, treatment, and human compliance on COVID-19 transmission. The homotopy perturbation method has also been successfully applied to study other viral infections, including equine infectious anemia virus (EIAV) [13] and hepatitis B virus [9], demonstrating its effectiveness in addressing both linear and nonlinear models.

The dynamics of diseases such as COVID-19 have prompted extensive investigations in the realm of epidemiological modeling. Ayoola et al. [12] presented a mathematical model for COVID-19 transmission that incorporates double-dose vaccination strategies, providing insights into effective containment measures. Additionally, Kolawole et al. [18] explored the effects of saturation terms on the SEIR epidemic model, highlighting the complexity of disease spread in populations with varying susceptibility.

Ayoola et al. [11] further developed the understanding of how enlightenment acceptance impacts disease transmission, applying the homotopy perturbation method to reveal critical factors influencing the spread of COVID-19. Complementing these studies, numerous investigations have revisited and extended mathematical models to adapt to the evolving nature of the pandemic. Similarly, Ndarou et al. [20] developed a compartmental model focusing on super-spreaders, calculating the basic reproduction number and demonstrating the models accuracy through numerical simulations of the COVID-19 outbreak in Wuhan, China. These efforts underscore the significance of mathematical modeling in informing vaccination strategies and managing the virus's spread.

There has been growing interest in using advanced mathematical tools and numerical methods to better understand and manage the spread of infectious diseases. As epidemics continue to pose serious public health challenges, researchers have developed and applied robust techniques to analyze the complex biological systems that underlie disease transmission. For example, the quasilinearization-Lagrangian method has been effectively used to explore the dynamics of HIV infection in CD4+ T cells, offering valuable insights into viral replication and the immune response [26]. Likewise, the shifted Boubaker Lagrangian approach has shown considerable promise in solving nonlinear biological models, thanks to its flexibility and precision in approximating analytical results [27]. Additionally, the pseudospectral Legendre method has emerged as a powerful tool for tackling time-dependent problems, particularly in modeling the progression of diseases like HIV [1]. These advances highlight the expanding role of fractional calculus and spectral techniques in capturing the real-world behavior of infectious diseases and improving the reliability of epidemiological models. Despite these advancements, a pressing need remains to integrate vaccination control elements within established models to assess their effectiveness in mitigating transmission. In response to this urgency, our study revisits and extends a previously established model by introducing a vaccination control factor. This adaptation aims to evaluate the potential impacts of frequent vaccine administration on the spread of COVID-19. To achieve this, we employ the Homotopy Perturbation Method to explore the criteria for the existence of numerical solutions, leveraging its effectiveness in analyzing complex systems [16, 2].

The aim of this study is to enhance the understanding of COVID-19 dynamics by analyzing the role of vaccination in disease transmission and recovery. Our research not only bridges the gap between theoretical modeling and practical public health strategies but also provides valuable insights that can inform evidence-based decision-making in the ongoing global battle against the pandemic. By highlighting the significant effects of the vaccination control factor on both the susceptible and recovery classes, this study contributes to our collective understanding of effective COVID-19 mitigation strategies.

1.1. Homotopy Perturbation Method

According to [17], the methodology of the HPM begins by considering the following differential equation:

$$D(\varpi) = g(\upsilon), \quad \upsilon \in \Phi. \tag{1}$$

Subject to the boundary condition:

$$\psi(\varpi, \varpi_n) = 0, \quad \upsilon \in \Pi. \tag{2}$$

The differential operator D acts on the analytic function $g(\upsilon)$. The boundary operator is represented by ψ, and the external normal vector derivative, denoted by ϖ_n, is derived from the domain Φ. The boundary of the domain is denoted by Π.
The operator $D(\varpi)$ is composed of linear and nonlinear parts such that:

$$D(\varpi) = Q_T(\varpi) + \mu_T(\varpi). \tag{3}$$

Thus, we have:

$$Q_T(\varpi) + \mu_T(\varpi) = g(\upsilon), \quad \varpi \in \Phi. \tag{4}$$

We can construct a Homotopy for equation (4) as follows:

$$\xi(\zeta, p) = (1-p)\left[Q_T(\zeta) - Q_T(\varpi_0)\right] + p\left[D(\zeta) - g(\upsilon)\right] = 0. \tag{5}$$

Here, $p \in [0, 1]$ is an embedding parameter. Expanding equation (5) yields:

$$\xi(\zeta, p) = Q_T(\zeta) - Q_T(\varpi_0) + p\left[Q_T(\varpi_0) + \mu_T(\varpi_0) - g(\upsilon)\right] = 0. \tag{6}$$

As $p \to 0$, equation (6) simplifies to:

$$\xi(\zeta, 0) = Q_T(\zeta) - Q_T(\varpi_0) = 0. \tag{7}$$

When $p \to 1$, it becomes:

$$\xi(\zeta, 1) = D(\zeta) - g(\upsilon) = 0. \tag{8}$$

The solution to equation (8) can be obtained iteratively by assuming a power series expansion in p:

$$\zeta(t) = \zeta_0(t) + p\zeta_1(t) + p^2\zeta_2(t) + \cdots + p^n\zeta_n(t). \tag{9}$$

Evaluating $\xi(\zeta, 1)$ using equation (9), we compare the coefficients of equal powers of p and subsequently solve to obtain the values of $\zeta_0(t)$, $\zeta_1(t)$, and $\zeta_2(t)$. The approximate solution of equation (8) is given by:

$$\zeta(t) = \lim_{p\to 1} \zeta_n(t) = \zeta_0(t) + \zeta_1(t) + \zeta_2(t) + \cdots . \tag{10}$$

2. Model Description

Consider $N(t)$ as the overall human population, which is further categorized into six classes: susceptible individuals $S(t)$, exposed individuals $E(t)$, asymptomatic infected individuals $I_A(t)$, symptomatic infected individuals $I_S(t)$, quarantined individuals $Q(t)$, and individuals who have recovered from Covid-19 $R(t)$. We present a compartmental-based model for analyzing the dynamics of COVID-19 disease, using the following system of ordinary differential equations (ODEs), given by (11) and graphically represented in Figure 1.

$$\begin{aligned}
\frac{dS(t)}{dt} &= \Lambda(1 - \alpha V_C) - (\tau + \mu)S(t) - \beta S(t)E(t) + \rho R(t),\\
\frac{dE(t)}{dt} &= \beta S(t)E(t) - (\gamma + \mu + \eta + \sigma)E(t),\\
\frac{dQ(t)}{dt} &= \tau S(t) + \gamma E(t) - (\mu + \upsilon + \theta)Q(t),\\
\frac{dI_A(t)}{dt} &= \sigma E(t) + \theta Q(t) - (\mu + r_1)I_A(t),\\
\frac{dI_S(t)}{dt} &= \eta E(t) + \upsilon Q(t) - (\delta + \mu + r_2)I_S(t),\\
\frac{dR(t)}{dt} &= \Lambda\alpha V_C + r_1 I_A(t) + r_2 I_S(t) - (\mu + \rho)R(t).
\end{aligned} \tag{11}$$

The system is subject to the following initial conditions:

$$S(0) = s_0, \quad E(0) = e_0, \quad Q(0) = q_0, \quad I_A(0) = i_0, \quad I_S(0) = i_0, \quad R(0) = r_0,$$

with the total human population given by:

$$N(t) = S(t) + E(t) + Q(t) + I_A(t) + I_S(t) + R(t). \tag{12}$$

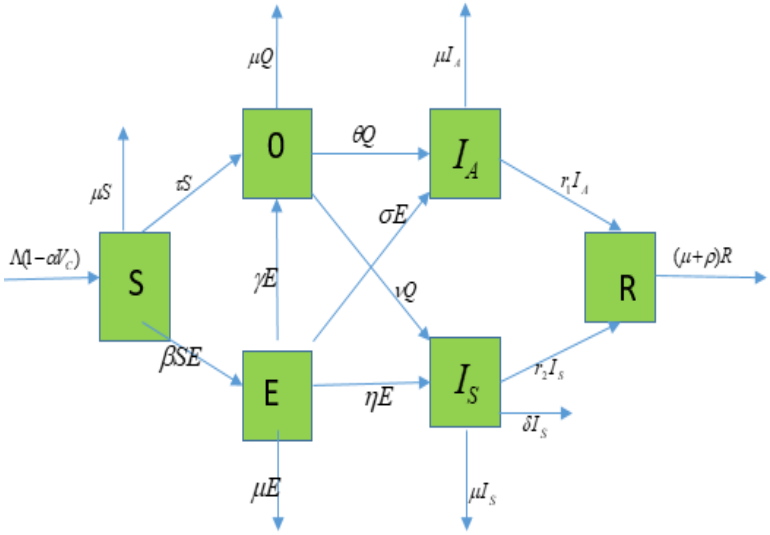

Figure 1. Schematic flow of the model

Table 1. Model nomenclatures, description and values

Description	Parameter	Value
Transfer rate from susceptible individuals to quarantine	τ	0.2×10^{-3}
Contact rate between susceptible and exposed individuals	β	0.805×10^{-4}
Fitted Mortality rate due to coronavirus in symptomatic infected individuals	δ	0.1×10^{-4}
Control factor	α	0.3×10^{-3}
Rate of transfer of exposed individuals to quarantine	γ	0.2×10^{-3}
Transfer rate from exposed individuals to symptomatic infected	η	0.478×10^{-2}
Rate of transfer of quarantine to asymptomatic infected individuals	θ	0.101×10^{-1}
Natural mortality rate	μ	0.106×10^{-1}
Fitted rate of transfer of quarantine to symptomatic infected individuals	υ	0.3×10^{-3}
Rate of transfer of exposed to asymptomatic infected individuals	σ	0.668×10^{-1}
Recruitment (natality) rate	Λ	200
Recovery rate of asymptomatic infected individuals	r_1	0.5×10^{-4}
Assumed recovery rate of symptomatic infected individuals	r_2	0.1×10^{-4}
Rate of transfer of vaccinated to recovered individuals	V_C	0.1×10^{-3}
Rate of transfer of recovered to susceptible individuals	ρ	0.5×10^{-2}
Initial susceptible population	$S(0)$	500
Initial exposed individuals	$E(0)$	2003
Initial quarantined individuals	$Q(0)$	2300
Initial asymptomatic infected individuals	$I_A(0)$	2000
Initial symptomatic infected individuals	$I_S(0)$	416
Initial recovered individuals	$R(0)$	155

2.1. Positivity and Boundedness

Theorem 1: Let Ω denote the region $0 \leq \alpha \leq \Omega$, then the equation has a unique solution. Since the human population in the model has been described, it is vital to show that the state parameters $S(t)$, $E(t)$, $Q(t)$, $I_A(t)$, $I_S(t)$, and $R(t)$ are non-negative for all $t \geq 0$. A solution with positive data remains positive for all $t \geq 0$ and is bounded. It is easy to see from the system that:

$$\Omega = \left\{ [S(t) + E(t) + Q(t) + I_A(t) + I_S(t) + R(t)] \in \mathbb{R}^{6+}; N(t) \leq \tfrac{\Lambda(1-\alpha V_c)}{\mu} \right\}$$

The total population at any point in time t is given by:

$$\tfrac{dN(t)}{dt} = \tfrac{d}{dt}\left[S(t) + E(t) + Q(t) + I_A(t) + I_S(t) + R(t)\right]$$
$$\tfrac{dN(t)}{dt} = \tfrac{dS}{dt} + \tfrac{dE}{dt} + \tfrac{dQ}{dt} + \tfrac{dI_A}{dt} + \tfrac{dI_S}{dt} + \tfrac{dR}{dt}$$

$$\begin{aligned} \tfrac{dN(t)}{dt} &= \left[\begin{array}{l} \Lambda(1-\alpha V_c) - (\tau+\mu)S - \beta SE + \rho R + \beta SE - (\gamma+\mu+\eta+\sigma)E + \tau S + \gamma E - (\mu+\nu+\theta)Q + \\ \sigma E + \theta Q - (\mu+r_1)I_A + \eta E + \nu\theta - (\delta+\mu+r_2)I_S + \Lambda\alpha V_c + r_1 I_A + r_2 I_S - (\mu+\rho)R \end{array} \right] \\ \tfrac{dN(t)}{dt} &= \Lambda - \delta I_S - \mu(S+E+Q+I_A+I_S+R) \\ \tfrac{dN(t)}{dt} &= \Lambda - \delta I_S - \mu N;\ \tfrac{dN(t)}{dt} + \mu N \leq \Lambda - \delta I_S \end{aligned} \tag{13}$$

Integrating the equation above yields:

$$N(t)e^{\mu t} = \frac{\Lambda - \delta I_S}{\mu} e^{\mu t} + C$$

where $C = N(0) - \frac{\Lambda - \delta I_S}{\mu}$. As C is a constant at the initial time t and for $N(t)$ such that

$$\lim_{t\to\infty} N(t) \leq \lim_{t\to\infty} \left[\frac{\Lambda - \delta I_S}{\mu} + \left(N(0) - \frac{\Lambda - \delta I_S}{\mu} \right) e^{\mu t} \right] = \frac{\Lambda - \delta I_S}{\mu},$$

we conclude that if $N(0) \leq \frac{\Lambda - \delta I_S}{\mu}$, then $N(t) \leq \frac{\Lambda - \delta I_S}{\mu}$.

Hence, it is sufficient to consider the dynamics of the model domain $\mathbb{R}^6_+$. In this region, the model can be considered to be mathematically and epidemiologically well posed.

2.2. Existence and Boundedness Theorem

The existence and boundedness of solutions to the proposed model are crucial for ensuring that the mathematical framework accurately represents the dynamics of the system being studied. By establishing these properties, we can guarantee that the solutions obtained from the model are valid and meaningful in the context of the underlying biological or epidemiological processes.

Theorem 1 *Let $g : \mathbb{R}^n \to \mathbb{R}^n$ be a continuously differentiable function defined as:*

$$\begin{aligned} g_1 &= \Lambda(1-\alpha V_c) - (\tau+\mu)S - \beta SE + \rho R, \\ g_2 &= \beta SE - (\gamma+\mu+\eta+\sigma)E, \\ g_3 &= \tau S + \gamma E - (\mu+\nu+\theta)Q, \\ g_4 &= \sigma E + \theta Q - (\mu+r_1)I_A, \\ g_5 &= \eta E + \nu\theta - (\delta+\mu+r_2)I_s, \\ g_6 &= \Lambda\alpha V_c + r_1 I_A + r_2 I_s - (\mu+\rho)R. \end{aligned} \tag{14}$$

If the partial derivatives of g exist and are continuous and bounded in $\mathbb{R}^6$, then the system of equations $g(x) = 0$ has a unique solution in $\mathbb{R}^6$.

Proof: To demonstrate the existence of a solution for the model, we will take the partial derivatives of the equations defined in g.

Let:

$$\begin{aligned} g_1 &= \Lambda(1-\alpha V_c) - (\tau+\mu)S - \beta SE + \rho R, \\ g_2 &= \beta SE - (\gamma+\mu+\eta+\sigma)E, \\ g_3 &= \tau S + \gamma E - (\mu+\nu+\theta)Q, \\ g_4 &= \sigma E + \theta Q - (\mu+r_1)I_A, \\ g_5 &= \eta E + \nu\theta - (\delta+\mu+r_2)I_s, \\ g_6 &= \Lambda\alpha V_c + r_1 I_A + r_2 I_s - (\mu+\rho)R. \end{aligned}$$

Thus, taking partial derivatives of these equations:

1. For g_1:

$$\left|\frac{\partial g_1}{\partial S}\right| = \tau+\mu+\beta < \infty, \quad \left|\frac{\partial g_1}{\partial E}\right| = \beta < \infty, \quad \left|\frac{\partial g_1}{\partial Q}\right| = 0 < \infty, \quad \left|\frac{\partial g_1}{\partial I_A}\right| = 0 < \infty, \quad \left|\frac{\partial g_1}{\partial I_s}\right| = 0 < \infty, \quad \left|\frac{\partial g_1}{\partial R}\right| = \rho < \infty.$$

2. For g_2:

$$\left|\frac{\partial g_2}{\partial S}\right| = \beta < \infty, \quad \left|\frac{\partial g_2}{\partial E}\right| = \beta + \gamma + \mu + \eta + \sigma < \infty, \quad \left|\frac{\partial g_2}{\partial Q}\right| = 0 < \infty, \quad \left|\frac{\partial g_2}{\partial I_A}\right| = 0 < \infty, \quad \left|\frac{\partial g_2}{\partial I_s}\right| = 0 < \infty, \quad \left|\frac{\partial g_2}{\partial R}\right| = 0 < \infty.$$

3. For g_3:

$$\left|\frac{\partial g_3}{\partial S}\right| = \tau < \infty, \quad \left|\frac{\partial g_3}{\partial E}\right| = \gamma < \infty, \quad \left|\frac{\partial g_3}{\partial Q}\right| = \mu + \nu + \theta < \infty, \quad \left|\frac{\partial g_3}{\partial I_A}\right| = 0 < \infty, \quad \left|\frac{\partial g_3}{\partial I_s}\right| = 0 < \infty, \quad \left|\frac{\partial g_3}{\partial R}\right| = 0 < \infty.$$

4. For g_4:

$$\left|\frac{\partial g_4}{\partial S}\right| = 0 < \infty, \quad \left|\frac{\partial g_4}{\partial E}\right| = \sigma < \infty, \quad \left|\frac{\partial g_4}{\partial Q}\right| = \theta < \infty, \quad \left|\frac{\partial g_4}{\partial I_A}\right| = \mu + r_1 < \infty, \quad \left|\frac{\partial g_4}{\partial I_s}\right| = 0 < \infty, \quad \left|\frac{\partial g_4}{\partial R}\right| = 0 < \infty.$$

5. For g_5:

$$\left|\frac{\partial g_5}{\partial S}\right| = 0 < \infty, \quad \left|\frac{\partial g_5}{\partial E}\right| = \eta < \infty, \quad \left|\frac{\partial g_5}{\partial Q}\right| = \nu < \infty, \quad \left|\frac{\partial g_5}{\partial I_A}\right| = 0 < \infty, \quad \left|\frac{\partial g_5}{\partial I_s}\right| = \delta + \mu + r_2 < \infty, \quad \left|\frac{\partial g_5}{\partial R}\right| = 0 < \infty.$$

6. For g_6:

$$\left|\frac{\partial g_6}{\partial S}\right| = 0 < \infty, \quad \left|\frac{\partial g_6}{\partial E}\right| = 0 < \infty, \quad \left|\frac{\partial g_6}{\partial Q}\right| = 0 < \infty, \quad \left|\frac{\partial g_6}{\partial I_A}\right| = r_1 < \infty, \quad \left|\frac{\partial g_6}{\partial I_s}\right| = r_2 < \infty, \quad \left|\frac{\partial g_6}{\partial R}\right| = \mu + \rho < \infty.$$

The partial derivatives of these functions exist, are continuous, and are bounded. Therefore, by the continuity and boundedness conditions established, the system of equations $g(x) = 0$ exists and has a unique solution. It is well-posed in $\mathbb{R}^6$.

2.3. Existence of Disease-Free Equilibrium (DFE)

To determine the critical points, we set the differential equations to zero at the disease-free equilibrium. Specifically, at the equilibrium state where $I_A = I_S = E = 0$, the DFE can be characterized as follows:

$$\begin{aligned} DFE &= (S_0, E_0, Q_0, I_{A0}, I_{S0}, R_0) = (S_0, 0, 0, 0, 0, R_0) \\ DFE &= \left(S = \frac{\Lambda(\mu + \rho - \mu\alpha V_C)}{(\tau + \mu)(\mu + \rho)},\ E = 0,\ Q = 0,\ I_A = 0,\ I_S = 0,\ R = \frac{\Lambda\alpha V_C}{(\mu + \rho)}\right) \\ E_1 &= \left(\frac{\Lambda(\mu + \rho - \mu\alpha V_C)}{(\tau + \mu)(\mu + \rho)},\ 0,\ 0,\ 0,\ 0,\ \frac{\Lambda\alpha V_C}{(\mu + \rho)}\right) \end{aligned}$$

3. Basic Reproduction Number (R_0)

The basic reproduction number, denoted by R_0, is the expected value of the infection rate per time unit that occurs in a susceptible population, caused by an infected individual. It is defined as follows:

$$R_0 = \rho F V^{-1}$$

where:

- F is the rate of appearance of new infections in the compartment.
- V is the rate of transfer of individuals from one compartment to another.
- ρ is the spectral radius.
- R_0 is the dominant eigenvalue of FV^{-1}.

The matrices F and V are given by:

$$F = \begin{pmatrix} \beta S(t) & 0 & 0 & 0 \\ 0 & 0 & 0 & 0 \\ 0 & 0 & 0 & 0 \\ 0 & 0 & 0 & 0 \end{pmatrix}$$

Substituting $S(t) = S_0 = \frac{\Lambda(\mu+\rho-\mu\alpha V_C)}{(\tau+\mu)(\mu+\rho)}$, we get the Jacobian matrix of F at the Disease-Free Equilibrium (DFE):

$$F = \begin{pmatrix} \beta\frac{\Lambda(\mu+\rho-\mu\alpha V_C)}{(\tau+\mu)(\mu+\rho)} & 0 & 0 & 0 \\ 0 & 0 & 0 & 0 \\ 0 & 0 & 0 & 0 \\ 0 & 0 & 0 & 0 \end{pmatrix}$$

Also, the matrix V is given by:

$$V = \begin{pmatrix} -(\gamma+\mu+\eta+\sigma)E(t) \\ \tau S(t)+\gamma E(t)-(\mu+\upsilon+\theta)Q(t) \\ \sigma E(t)+\theta(t)Q-(\mu+r_1)I_A(t) \\ \eta E(t)-\upsilon Q(t)-(\delta+\mu+r_2)I_S(t) \end{pmatrix}$$

The Jacobian matrix of V at DFE is:

$$V = \begin{pmatrix} -(\gamma+\mu+\eta+\sigma) & 0 & 0 & 0 \\ \gamma & -(\mu+\upsilon+\theta) & 0 & 0 \\ \sigma & \theta & -(\mu+r_1) & 0 \\ \eta & \upsilon & 0 & -(\delta+\mu+r_2) \end{pmatrix}$$

Define the following parameters:

$$\begin{aligned} a &= -(\gamma+\mu+\eta+\sigma) \\ b &= -(\mu+\upsilon+\theta) \\ c &= -(\mu+r_1) \\ d &= -(\delta+\mu+r_2) \\ e &= -(\tau+\mu) \\ f &= -(\mu+\rho) \\ g &= -\alpha V_C \mu \end{aligned}$$

Thus, the inverse of V is given by:

$$V^{-1} = \begin{pmatrix} \frac{1}{a} & 0 & 0 & 0 \\ -\frac{\gamma}{ab} & \frac{1}{b} & 0 & 0 \\ \frac{\gamma\theta-\sigma b}{abc} & -\frac{\theta}{bc} & \frac{1}{c} & 0 \\ \frac{\gamma\upsilon-b\eta}{abd} & -\frac{\upsilon}{bd} & 0 & \frac{1}{d} \end{pmatrix}$$

Finally, the basic reproduction number is:

$$R_0 = FV^{-1}$$

$$R_0 = \begin{pmatrix} \beta S(t) & 0 & 0 & 0 \\ 0 & 0 & 0 & 0 \\ 0 & 0 & 0 & 0 \\ 0 & 0 & 0 & 0 \end{pmatrix} \begin{pmatrix} \frac{1}{a} & 0 & 0 & 0 \\ -\frac{\gamma}{ab} & \frac{1}{b} & 0 & 0 \\ \frac{\gamma\theta-\sigma b}{abc} & -\frac{\theta}{bc} & \frac{1}{c} & 0 \\ \frac{\gamma\upsilon-b\eta}{abd} & -\frac{\upsilon}{bd} & 0 & \frac{1}{d} \end{pmatrix} \tag{15}$$

Where $S_0 = \frac{\Lambda(\mu+\rho-\mu\alpha V_C)}{(\tau+\mu)(\mu+\rho)}$ and $a = -(\gamma+\mu+\eta+\sigma)$
Substituting into Equation (15) we have

$$R_0 = \begin{pmatrix} \beta\frac{\Lambda(\mu+\rho-\mu\alpha V_C)}{(\tau+\mu)(\mu+\rho)} & 0 & 0 & 0 \\ \overline{-(\gamma+\mu+\eta+\sigma)} & 0 & 0 & 0 \\ 0 & 0 & 0 & 0 \\ 0 & 0 & 0 & 0 \\ 0 & 0 & 0 & 0 \end{pmatrix} = \begin{pmatrix} -\frac{\beta\Lambda(\mu+\rho-\mu\alpha V_C)}{(\tau+\mu)(\mu+\rho)(\gamma+\mu+\eta+\sigma)} & 0 & 0 & 0 \\ 0 & 0 & 0 & 0 \\ 0 & 0 & 0 & 0 \\ 0 & 0 & 0 & 0 \end{pmatrix} \tag{16}$$

$$\rho_1(FV^{-1}) = -\frac{\beta\Lambda(\mu+\rho-\mu\alpha V_C)}{(\tau+\mu)(\mu+\rho)(\gamma+\mu+\eta+\sigma)} = R_0$$

Where ρ_1 is the spectral radius of the next generation matrix FV^{-1}:

$$R_0 = -\frac{\beta\Lambda(\mu+\rho-\mu\alpha V_C)}{(\tau+\mu)(\mu+\rho)(\gamma+\mu+\eta+\sigma)}$$

4. Local Stability Analysis of the Disease-Free Equilibrium (DFE)

Theorem 2: The disease-free state of the model is locally asymptotically stable if the threshold for disease spread is less than one ($R_0 < 1$), and it becomes unstable when this threshold exceeds one ($R_0 > 1$).
Proof: The Jacobian matrix corresponding to system (10) is given by

$$J = \begin{pmatrix} -(\tau+\mu)-\beta E & -\beta S & 0 & 0 & 0 & \rho \\ \beta E & \beta S-(\gamma+\mu+\eta+\sigma) & 0 & 0 & 0 & 0 \\ \tau & \gamma & -(\mu+\upsilon+\theta) & 0 & 0 & 0 \\ 0 & \sigma & \theta & -(\mu+r_1) & 0 & 0 \\ 0 & \eta & \upsilon & 0 & -(\delta+\mu+r_2) & 0 \\ 0 & 0 & 0 & r_1 & r_2 & -(\mu+\rho) \end{pmatrix}$$

At DFE, $E^* = Q^* = I_A^* = I_S^* = R^* = 0$ and

$$S_0 = \frac{\Lambda(\mu+\rho-\mu\alpha V_C)}{(\tau+\mu)(\mu+\rho)}$$

which implies

$$J_{DFE} = \begin{pmatrix} -(\tau+\mu) & -\beta\left(\frac{\Lambda(\mu+\rho-\mu\alpha V_C)}{(\tau+\mu)(\mu+\rho)}\right) & 0 & 0 & 0 & \rho \\ 0 & \beta\left(\frac{\Lambda(\mu+\rho-\mu\alpha V_C)}{(\tau+\mu)(\mu+\rho)}\right)-(\gamma+\mu+\eta+\sigma) & 0 & 0 & 0 & 0 \\ \tau & \gamma & -(\mu+\upsilon+\theta) & 0 & 0 & 0 \\ 0 & \sigma & \theta & -(\mu+r_1) & 0 & 0 \\ 0 & \eta & \upsilon & 0 & -(\delta+\mu+r_2) & 0 \\ 0 & 0 & 0 & r_1 & r_2 & -(\mu+\rho) \end{pmatrix}$$

For easy simplification, let

$$\begin{aligned} a &= -(\gamma+\mu+\eta+\sigma), \\ b &= -(\mu+\upsilon+\theta), \\ c &= -(\mu+r_1), \\ d &= -(\delta+\mu+r_2), \\ e &= -(\tau+\mu), \\ f &= -(\mu+\rho), \\ g &= -\alpha V_C \mu. \end{aligned}$$

Thus,

$$J_{DFE} = \begin{pmatrix} e & \beta\left(\frac{\Lambda(f-g)}{ef}\right) & 0 & 0 & 0 & \rho \\ 0 & \beta\left(\frac{\Lambda(g-f)}{ef}\right)+a & 0 & 0 & 0 & 0 \\ \tau & \gamma & b & 0 & 0 & 0 \\ 0 & \sigma & \theta & c & 0 & 0 \\ 0 & \eta & \upsilon & 0 & d & 0 \\ 0 & 0 & 0 & r_1 & r_2 & f \end{pmatrix}$$

The characteristic polynomial of the Jacobian matrix of Disease Free Equilibrium is given by

$$\mathbf{Det}(J_{DFE} - \boldsymbol{\lambda} I)$$

where $\boldsymbol{\lambda}$ is the eigenvalue and I is the identity matrix.
To give

$$J_{DFE} - \lambda I = \begin{pmatrix} e-\lambda_1 & \beta\left(\frac{\Lambda(f-g)}{ef}\right) & 0 & 0 & 0 & \rho \\ 0 & \beta\left(\frac{\Lambda(g-f)}{ef}\right)+a-\lambda_2 & 0 & 0 & 0 & 0 \\ \tau & \gamma & b-\lambda_3 & 0 & 0 & 0 \\ 0 & \sigma & \theta & c-\lambda_4 & 0 & 0 \\ 0 & \eta & \upsilon & 0 & d-\lambda_5 & 0 \\ 0 & 0 & 0 & r_1 & r_2 & f-\lambda_6 \end{pmatrix}$$

Computing the eigenvalues of ((3.28),

$$\begin{aligned} &\lambda_1 = -(\tau+\mu) < 0,\ \lambda_2 = -(\gamma+\mu+\eta+\sigma) < 0,\ \lambda_3 = -(\mu+\upsilon+\theta) < 0, \\ &\lambda_4 = -(\mu+r_1) < 0,\ \lambda_5 = -(\delta+\mu+r_2) < 0\,,\ \lambda_6 = -(\tau+\mu) < 0, \end{aligned}$$

Since all the Eigen values are negatively invariant and R_0<1, then the Disease free Equilibrium (DFE) is locally asymptotically stable.
This completes the proof.

5. Numerical Solution via HPM

In this section, the homotopy perturbation method is applied to obtain the approximate solution of the system of differential equations in (17).

$$\begin{aligned}
\tfrac{dS(t)}{dt} &= \Lambda(1-\alpha V_C) - (\tau+\mu)S(t) - \beta S(t)E(t) + \rho R \\
\tfrac{dE(t)}{dt} &= \beta S(t)E(t) - (\gamma+\mu+\eta+\sigma)E(t) \\
\tfrac{dQ(t)}{dt} &= \tau S(t) + \gamma E(t) - (\mu+\upsilon+\theta)Q(t) \\
\tfrac{dI_A(t)}{dt} &= \sigma E(t) + \theta Q(t) - (\mu+r_1)I_A(t) \\
\tfrac{dI_S(t)}{dt} &= \eta E(t) + \upsilon Q(t) - (\delta+\mu+r_2)I_S(t) \\
\tfrac{dR(t)}{dt} &= \Lambda\alpha V_C + r_1 I_A(t) + r_2 I_S(t) - (\mu+\rho)R(t)
\end{aligned} \tag{17}$$

Subject to initial conditions: $S(0)=s_0, E(0)=e_0, Q(0)=q_0, I_A(0)=i_{A0}, I_S(0)=i_{S0}, R(0)=r_0$.
The following system of power series is assumed to be the solution to the problem:

$$S(t) = s_0(t) + ps_1(t) + p^2 s_2(t) + \dots$$

$$E(t) = e_0(t) + pe_1(t) + p^2 e_2(t) + \dots$$

$$Q(t) = q_0(t) + pq_1(t) + p^2 q_2(t) + \dots$$

$$I_A(t) = i_{A0}(t) + pi_{A1}(t) + p^2 i_{A2}(t) + \dots$$

$$I_S(t) = i_{S0}(t) + pi_{S1}(t) + p^2 i_{S2}(t) + \dots$$

$$R(t) = r_0(t) + pr_1(t) + p^2 r_2(t) + \dots$$

Here, the algorithm discussed in the methodology shall be applied to solve the proposed system. This is initiated by constructing the following correctional functional, given by

$$(1-P)\tfrac{dS}{dt} + P\left[\tfrac{dS}{dt} - (\Lambda(1-\alpha V_C) - (\tau+\mu)S - \beta SE + \rho R)\right]$$

$$(1-P)\tfrac{dE}{dt} + P\left[\tfrac{dE}{dt} - (\beta SE - (\gamma+\mu+\eta+\sigma)E)\right]$$

$$(1-P)\tfrac{dQ}{dt} + P\left[\tfrac{dQ}{dt} - (\tau S + \gamma E - (\mu+\upsilon+\theta)Q)\right]$$

$$(1-P)\tfrac{dI_A}{dt} + P\left[\tfrac{dI_A}{dt} - (\sigma E + \theta Q - (\mu+r_1)I_A)\right]$$

$$(1-P)\tfrac{dI_S}{dt} + P\left[\tfrac{dI_S}{dt} - (\eta E + \upsilon Q - (\delta+\mu+r_2)I_S)\right]$$

$$(1-P)\tfrac{dR}{dt} + P\left[\tfrac{dR}{dt} - (\Lambda\alpha V_C + r_1 I_A + r_2 I_S - (\mu+\rho)R)\right]$$

For P^0:

$$\frac{dS_0(t)}{dt} = 0, \quad \frac{dE_0(t)}{dt} = 0, \quad \frac{dQ_0(t)}{dt} = 0, \quad \frac{dI_{A0}(t)}{dt} = 0, \quad \frac{dI_{S0}(t)}{dt} = 0, \quad \frac{dR_0(t)}{dt} = 0$$

Solving the above equations, we obtain

$$s_0(t) = s_0, \quad e_0(t) = e_0, \quad q_0(t) = q_0, \quad i_{A0}(t) = i_{A0}, \quad i_{S0}(t) = i_{S0}, \quad r_0(t) = r_0$$

Also, the coefficient of p^1 is given as:

$$\begin{aligned}
\tfrac{dS_0}{dt} &= (\Lambda(1-\alpha V_c) - (\tau+\mu)S_0 - \beta S_0 E_0 + \rho R_0) \\
\tfrac{dE_0}{dt} &= (\beta S_0 E_0 - (\gamma+\mu+\eta+\sigma)E_0) \\
\tfrac{dQ_0}{dt} &= (\tau S_0 + \gamma E_0 - (\mu+\upsilon+\theta)Q_0) \\
\tfrac{dI_{A0}}{dt} &= (\sigma E_0 + \theta Q_0 - (\mu+r_1)I_{A0}) \\
\tfrac{dI_{S0}}{dt} &= (\eta E_0 + \upsilon Q_0 - (\delta+\mu+r_2)I_S) \\
\tfrac{dR_0}{dt} &= (\Lambda\alpha V_c + r_1 I_{A0} + r_2 I_{S0} - (\mu+\rho)R_0)
\end{aligned} \tag{18}$$

Solving this system of equations yields:

$$s_1(t) = (-\tau s_0 + \Lambda - \beta s_0 e_0 - \Lambda\alpha V_c + \rho r_0 - \mu s_0)\, t$$

$$e_1(t) = -e_0(\gamma+\mu+\eta+\sigma-\beta s_0)\, t$$

$$q_1(t) = (-\theta q_0 + \tau s_0 - \nu q_0 - \mu q_0 + \gamma e_0)\, t$$

$$i_a(t) = (\theta q_0 + \sigma e_0 - i_{a0} z - \mu i_{a0})\, t$$

$$i_s(t) = (-i_{s0} k + \eta e_0 - \mu i_{s0} - \delta i_{s0} + \nu q_0)\, t$$

$$r_1(t) = (-\mu r_0 + \Lambda\alpha V_c + i_{a0} z - \rho r_0 + i_{s0} k)\, t$$

Similarly, comparing the coefficient of p^2 is given as :

$$\begin{aligned}
&\tfrac{d}{dt}s_2(t) + \mu s_1(t) + \tau s_1(t) + \beta s_0(t)e_1(t) - \rho r_1(t) + \beta s_1(t)e_0(t) = 0 \\
&\tfrac{d}{dt}e_2(t) - \beta s_1(t)e_0(t) + \gamma e_1(t) + \sigma e_1(t) + \eta e_1(t) + \mu e_1(t) - \beta s_0(t)e_1(t) = 0 \\
&\tfrac{d}{dt}q_2(t) - \gamma e_1(t) - \tau s_1(t) + \nu q_1(t) + \mu q_1(t) + \theta q_1(t) = 0 \\
&\tfrac{d}{dt}i_{a_2}(t) - \theta q_1(t) - \sigma e_1(t) + z i_{a_1}(t) + \mu i_{a_1}(t) = 0 \\
&\tfrac{d}{dt}i_{s_2}(t) - \nu q_1(t) - \eta e_1(t) + \mu i_{s_1}(t) + \delta i_{s_1}(t) + r_2 i_{s_1}(t) = 0 \\
&\tfrac{d}{dt}r_2(t) - k i_{s_1}(t) - z i_{a_1}(t) + \rho r_1(t) + \mu r_1(t) = 0
\end{aligned} \tag{19}$$

In solving this system of differential equations:

$$\begin{aligned}
s_2(t) = \tfrac{1}{2}t^2 &(-2r_0\rho\mu + 2\mu\tau s_0 + V_c\alpha\Lambda\mu - r_0\rho\tau + V_c\alpha\Lambda\tau \\
&- \beta^2 s_0^2 e_0 - \Lambda V_c\alpha\rho + i_{a0}z\rho + i_{s0}k\rho + \beta^2 e_0^2 s_0 - \beta e_0\Lambda + 3\mu s_0\beta e_0 + 2\tau s_0\beta e_0 + \beta s_0 e_0\sigma + \beta s_0 e_0\gamma + \beta s_0 e_0\eta \\
&- \beta e_0\rho r_0 + \beta e_0 V_c\Lambda - \Lambda\mu + \mu^2 s_0 + \tau^2 s_0 - \Lambda\tau - r_0\rho^2)
\end{aligned}$$

$$\begin{aligned}
e_2(t) = -\tfrac{1}{2}e_0 t^2 &(\beta^2 e_0 s_0 - \beta^2 s_0^2 + \beta\tau s_0 - \beta\Lambda - 2\mu\gamma - 2\sigma\gamma - 2\eta\gamma \\
&-2\sigma\mu - 2\eta\sigma - 2\eta\mu - \gamma^2 + \sigma^2 - \eta^2 - \mu^2 + 3\beta\mu s_0 - \beta\rho r_0 + 2\beta s_0\sigma - 2\beta s_0\gamma - 2\beta s_0\eta - \beta V_c\alpha\Lambda)
\end{aligned}$$

$$\begin{aligned}
q_2(t) = -\tfrac{1}{2}t^2 &(2\mu\tau s_0 - r_0\rho\tau + V_c\alpha\Lambda\tau - q_0\nu^2 - q_0\mu^2 - q_0\theta^2 + 2\gamma e_0\mu + \gamma e_0\sigma \\
&+\gamma e_0\eta + \gamma^2 e_0 - 2q_0\theta\nu + \nu\tau s_0 - 2q_0\mu\nu + \nu\gamma e_0 - 2q_0\theta\mu + s_0\tau\theta + \theta\gamma e_0 + \tau s_0\beta e_0 - \beta s_0 e_0\gamma + \tau^2 s_0 - \Lambda\tau)
\end{aligned}$$

$$\begin{aligned}
i_{a2}(t) = -\tfrac{1}{2}t^2 &(\theta^2 q_0 - s_0\tau\theta + q_0\theta\nu - 2q_0\theta\mu - \gamma e_0\theta - \beta s_0 e_0\sigma \\
&+2\mu e_0\sigma + \sigma^2 e_0 + \gamma e_0\sigma + \sigma e_0\eta + z q_0\theta + z e_0\sigma - i_{a0}z^2 - 2i_{a0}\mu z - u^2 i_{a0})
\end{aligned}$$

$$\begin{aligned}
i_{s2}(t) = -\tfrac{1}{2}t^2 &(-i_{s0}u^2 - i_{s0}\delta^2 - i_{s0}k\mu - 2i_{s0}\delta\mu - i_{s0}k\delta + \delta\eta e_0 \\
&+ \delta\nu q_0 - i_{s0}kr_2 + r_2\eta e_0 - \mu i_{s0}r_2 - r_2\delta i_{s0} + r_2\nu q_0 + \nu^2 q_0 + \gamma\eta e_0 + \sigma\eta e_0 + 2\eta e_0\mu + \eta^2 e_0 + q_0\theta\nu - s_0\tau\nu - 2\nu q_0\mu - \nu\gamma e_0 - \beta s_0 e_0\eta)
\end{aligned}$$

$$r_2(t) = \frac{1}{2}t^2\left(-i_{s0}k^2 + ke_0\eta - 2k\mu i_{s0} - k\delta i_{s0} + kvq_0 + zq_0\theta + z\sigma e_0 + i_{a0}z^2 - 2i_{a0}\mu z + 2r_0\mu\rho + \alpha V_c\Lambda\rho + zi_{a0}\rho + \rho^2 r_0 - \rho k i_{s0} + r_0\mu^2 - \Lambda\alpha V_c\mu\right)$$

The solution for each class is obtained by summing its respective approximations.
Such that

$$S(t) = \sum_{n=0}^{2} s_n(t), E(t) = \sum_{n=0}^{2} e_n(t), Q(t) = \sum_{n=0}^{2} q_n(t), I_a(t) = \sum_{n=0}^{2} i_{an}(t), I_s(t) = \sum_{n=0}^{2} i_{sn}(t), R(t) = \sum_{n=0}^{2} r_n(t). \tag{20}$$

6. Special solution by Laplace Adomian decomposition method

To apply the LADM to solve system (11) , we take the Laplace transform of both sides of the system. Recall that $\mathscr{L}\left[\frac{dy}{dt}\right] = s\mathscr{L}[y(t)] - y(0)$. Hence, we have:

$$\begin{aligned}
\mathscr{L}\left[\frac{dS}{dt}\right] &= \mathscr{L}\left[\Lambda(1-\alpha V_C) - (\gamma+\mu)S(t) - \beta S(t)E(t) + \rho R(t)\right],\\
\mathscr{L}\left[\frac{dE}{dt}\right] &= \mathscr{L}\left[\beta S(t)E(t) - (\gamma+\mu+\eta+\sigma)E(t)\right],\\
\mathscr{L}\left[\frac{dQ}{dt}\right] &= \mathscr{L}\left[\tau S(t) + \gamma E(t) - (\mu+v+\theta)Q(t)\right],\\
\mathscr{L}\left[\frac{dI_A}{dt}\right] &= \mathscr{L}\left[\sigma E(t) + \theta Q(t) - (\mu+n)I_A(t)\right],\\
\mathscr{L}\left[\frac{dI_S}{dt}\right] &= \mathscr{L}\left[\eta E(t) + vQ(t) - (\delta+\mu+r_2)I_S(t)\right],\\
\mathscr{L}\left[\frac{dR}{dt}\right] &= \mathscr{L}\left[\Lambda\alpha V_C + nI_A(t) + r_2 I_S(t) - (\mu+\rho)R(t)\right].
\end{aligned} \tag{21}$$

This simplifies to:

$$\begin{aligned}
s\mathscr{L}[S(t)] - S(0) &= \frac{\Lambda(1-\alpha V_C)}{s} - (\gamma+\mu)\mathscr{L}[S(t)] - \beta\mathscr{L}[S(t)E(t)] + \rho\mathscr{L}[R(t)],\\
s\mathscr{L}[E(t)] - E(0) &= \beta\mathscr{L}[S(t)E(t)] - (\gamma+\mu+\eta+\sigma)\mathscr{L}[E(t)],\\
s\mathscr{L}[Q(t)] - Q(0) &= \tau\mathscr{L}[S(t)] + \gamma\mathscr{L}[E(t)] - (\mu+v+\theta)\mathscr{L}[Q(t)],\\
s\mathscr{L}[I_A(t)] - I_A(0) &= \sigma\mathscr{L}[E(t)] + \theta\mathscr{L}[Q(t)] - (\mu+n)\mathscr{L}[I_A(t)],\\
s\mathscr{L}[I_S(t)] - I_S(0) &= \eta\mathscr{L}[E(t)] + v\mathscr{L}[Q(t)] - (\delta+\mu+r_2)\mathscr{L}[I_S(t)],\\
s\mathscr{L}[R(t)] - R(0) &= \frac{\Lambda\alpha V_C}{s} + n\mathscr{L}[I_A(t)] + r_2\mathscr{L}[I_S(t)] - (\mu+\rho)\mathscr{L}[R(t)].
\end{aligned} \tag{22}$$

Rearrange each equation to solve for $\mathscr{L}[S(t)]$, $\mathscr{L}[E(t)]$, $\mathscr{L}[Q(t)]$, $\mathscr{L}[I_A(t)]$, $\mathscr{L}[I_S(t)]$, $\mathscr{L}[R(t)]$:

$$\begin{aligned}
\mathscr{L}[S(t)] &= \frac{S(0)}{s} + \frac{\Lambda(1-\alpha V_C)}{s^2} - \frac{(\gamma+\mu)}{s}\mathscr{L}[S(t)] - \frac{\beta}{s}\mathscr{L}[S(t)E(t)] + \frac{\rho}{s}\mathscr{L}[R(t)],\\
\mathscr{L}[E(t)] &= \frac{E(0)}{s} + \frac{\beta}{s}\mathscr{L}[S(t)E(t)] - \frac{(\gamma+\mu+\eta+\sigma)}{s}\mathscr{L}[E(t)],\\
\mathscr{L}[Q(t)] &= \frac{Q(0)}{s} + \frac{\tau}{s}\mathscr{L}[S(t)] + \frac{\gamma}{s}\mathscr{L}[E(t)] - \frac{(\mu+v+\theta)}{s}\mathscr{L}[Q(t)],\\
\mathscr{L}[I_A(t)] &= \frac{I_A(0)}{s} + \frac{\sigma}{s}\mathscr{L}[E(t)] + \frac{\theta}{s}\mathscr{L}[Q(t)] - \frac{(\mu+n)}{s}\mathscr{L}[I_A(t)],\\
\mathscr{L}[I_S(t)] &= \frac{I_S(0)}{s} + \frac{\eta}{s}\mathscr{L}[E(t)] + \frac{v}{s}\mathscr{L}[Q(t)] - \frac{(\delta+\mu+r_2)}{s}\mathscr{L}[I_S(t)],\\
\mathscr{L}[R(t)] &= \frac{R(0)}{s} + \frac{\Lambda\alpha V_C}{s^2} + \frac{n}{s}\mathscr{L}[I_A(t)] + \frac{r_2}{s}\mathscr{L}[I_S(t)] - \frac{(\mu+\rho)}{s}\mathscr{L}[R(t)].
\end{aligned} \tag{23}$$

Express each variable as an infinite series:

$$S(t)=\sum_{n=0}^{\infty}S_n(t),\quad E(t)=\sum_{n=0}^{\infty}E_n(t),\quad Q(t)=\sum_{n=0}^{\infty}Q_n(t),$$
$$I_A(t)=\sum_{n=0}^{\infty}I_{A_n}(t),\quad I_S(t)=\sum_{n=0}^{\infty}I_{S_n}(t),\quad R(t)=\sum_{n=0}^{\infty}R_n(t). \tag{24}$$

For the nonlinear term $S(t)E(t)$, use the Adomian polynomials A_n:

$$S(t)E(t)=\sum_{n=0}^{\infty}A_n,\quad \text{where}\quad A_n=\sum_{k=0}^{n}S_k(t)E_{n-k}(t).$$

The initial approximations are derived from the initial conditions and the constant terms:

$$\begin{aligned}
S_0(t)&=\mathscr{L}^{-1}\left[\tfrac{S(0)}{s}+\tfrac{\Lambda(1-\alpha V_C)}{s^2}\right]=S(0)+\Lambda(1-\alpha V_C)t,\\
E_0(t)&=\mathscr{L}^{-1}\left[\tfrac{E(0)}{s}\right]=E(0),\\
Q_0(t)&=\mathscr{L}^{-1}\left[\tfrac{Q(0)}{s}\right]=Q(0),\\
I_{A_0}(t)&=\mathscr{L}^{-1}\left[\tfrac{I_A(0)}{s}\right]=I_A(0),\\
I_{S_0}(t)&=\mathscr{L}^{-1}\left[\tfrac{I_S(0)}{s}\right]=I_S(0),\\
R_0(t)&=\mathscr{L}^{-1}\left[\tfrac{R(0)}{s}+\tfrac{\Lambda\alpha V_C}{s^2}\right]=R(0)+\Lambda\alpha V_C t.
\end{aligned} \tag{25}$$

The recursive relations are used to compute $S_{n+1}(t)$, $E_{n+1}(t)$,$Q_{n+1}(t)$:

$$\begin{aligned}
S_{n+1}(t)&=\mathscr{L}^{-1}\left[-\frac{(\gamma+\mu)}{s}\mathscr{L}[S_n(t)]-\frac{\beta}{s}\mathscr{L}[A_n]+\frac{\rho}{s}\mathscr{L}[R_n(t)]\right],\\
E_{n+1}(t)&=\mathscr{L}^{-1}\left[\frac{\beta}{s}\mathscr{L}[A_n]-\frac{(\gamma+\mu+\eta+\sigma)}{s}\mathscr{L}[E_n(t)]\right],\\
Q_{n+1}(t)&=\mathscr{L}^{-1}\left[\frac{\tau}{s}\mathscr{L}[S_n(t)]+\frac{\gamma}{s}\mathscr{L}[E_n(t)]-\frac{(\mu+v+\theta)}{s}\mathscr{L}[Q_n(t)]\right],\\
I_{A_{n+1}}(t)&=\mathscr{L}^{-1}\left[\frac{\sigma}{s}\mathscr{L}[E_n(t)]+\frac{\theta}{s}\mathscr{L}[Q_n(t)]-\frac{(\mu+n)}{s}\mathscr{L}[I_{A_n}(t)]\right],\\
I_{S_{n+1}}(t)&=\mathscr{L}^{-1}\left[\frac{\eta}{s}\mathscr{L}[E_n(t)]+\frac{v}{s}\mathscr{L}[Q_n(t)]-\frac{(\delta+\mu+r_2)}{s}\mathscr{L}[I_{S_n}(t)]\right],\\
R_{n+1}(t)&=\mathscr{L}^{-1}\left[\frac{n}{s}\mathscr{L}[I_{A_n}(t)]+\frac{r_2}{s}\mathscr{L}[I_{S_n}(t)]-\frac{(\mu+\rho)}{s}\mathscr{L}[R_n(t)]\right].
\end{aligned} \tag{26}$$

The approximate solution is obtained by summing the initial and higher-order terms:

$$S(t)=\sum_{n=0}^{4}S_n(t),\quad E(t)=\sum_{n=0}^{4}E_n(t),\quad Q(t)=\sum_{n=0}^{4}Q_n(t),$$
$$I_A(t)=\sum_{n=0}^{4}I_{A_n}(t),\quad I_S(t)=\sum_{n=0}^{4}I_{S_n}(t),\quad R(t)=\sum_{n=0}^{4}R_n(t). \tag{27}$$

7. Results

Evaluating (20) and (27) using the numerical values of parameters in Table 1 respectively yields the polynomial solutions of HPM and LADM in (28) and (29):

$$\begin{aligned}
S_h(t)&=500+114.7542440\,t-8.178754620\,t^2+0.5809353103\,t^3,\\
E_h(t)&=2003-84.3863900\,t+11.02917252\,t^2-0.8543170867\,t^3,\\
Q_h(t)&=2300-47.7994\,t+0.5049304855\,t^2-0.003344485538\,t^3,\\
I_{A_h}(t)&=2000+135.73040\,t-3.782656775\,t^2+0.2607112723\,t^3,\\
I_{S_h}(t)&=416+5.84642\,t-0.2398978723\,t^2+0.01847287973\,t^3,\\
R_h(t)&=155-2.31383400\,t+0.02147039730\,t^2-0.0001754900052\,t^3.
\end{aligned} \tag{28}$$

and

$$\begin{aligned} S_L(t) &= 500 + 114.7542440\,t - 8.178754620\,t^2 + 0.5809353103\,t^3, \\ E_L(t) &= 2003 - 84.38639000\,t + 11.02917253\,t^2 - 0.8543170867\,t^3, \\ Q_L(t) &= 2300 - 47.79940000\,t + 0.5049304854\,t^2 - 0.003344485538\,t^3, \\ I_{A_L}(t) &= 2000 + 135.73040\,t - 3.782656777\,t^2 + 0.2607112725\,t^3, \\ I_{S_L}(t) &= 416 + 5.84642\,t - 0.2398978722\,t^2 + 0.01847287974\,t^3, \\ R_L(t) &= 155 - 2.313834000\,t + 0.02147039730\,t^2 - 0.0001754900051\,t^3. \end{aligned} \tag{29}$$

In similar fashion to [21, 5], the model solutions using both the Homotopy Perturbation Method (HPM) and Laplace Adomian Decomposition Method (LADM) yielded closely matching polynomial approximations for the compartments of the epidemic model, confirming the reliability of these analytical techniques. Over the time interval analyzed, the susceptible population increased from 500 to approximately 1295, suggesting net recruitment or births exceeding infection losses, this observation closely aligned with the outcome of [18]. The exposed class steadily declined from 2003 to 1784, reflecting progression to infectious or quarantined states. Similarly, the quarantined population decreased from 2300 to 2073, indicating recovery or release. In contrast, the asymptomatic infectious group grew notably from 2000 to 2602, signaling active disease transmission, while the symptomatic infectious increased modestly from 416 to 441. The recovered population showed a slight initial decline from 155 to 144, possibly due to delayed recoveries or demographic factors. These trends collectively illustrate the nonlinear disease dynamics captured by the model and highlight ongoing transmission alongside effective progression through disease stages.

Table 2. Population values at different time steps

Time Step	$S_h(t)$	$E_h(t)$	$Q_h(t)$	$I_{A_h}(t)$	$I_{S_h}(t)$	$R_h(t)$
1	500.0000000	2003.000000	2300.000000	2000.000000	416.000000	155.000000
2	617.3652905	1928.888516	2252.702168	2132.181578	421.623072	152.7074655
3	747.7670179	1872.922211	2206.393879	2257.999718	426.851257	150.4568825
4	900.5460036	1832.265915	2161.054421	2378.149991	431.733239	148.2473622
5	1081.882268	1804.102674	2116.662651	2492.870228	436.284953	146.0781246
6	1294.811849	1784.474741	2073.196996	2602.044565	440.497031	143.9484992

8. Numerical Simulations

In this section, we utilize Maple 18 software to perform numerical simulations on the mathematical model. The simulation examines the time variation of the effect of the control factor (α) on the susceptible class variables and the relapse rate of recovered individuals in the model. The results are given as Figures 2 to 5.

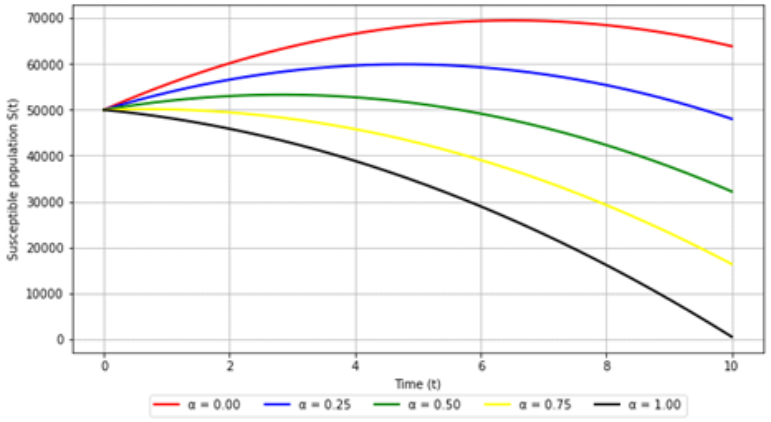

Figure 2. Impact of the control factor α on the Susceptible Class over time.

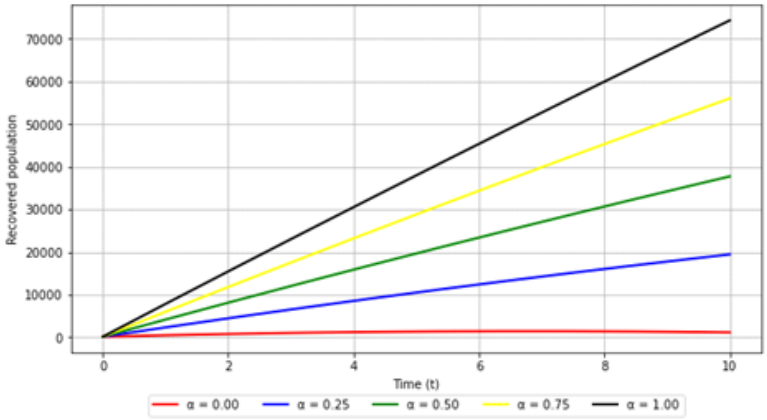

Figure 3. Influence of the control factor α on the Recovery Class as a function of time.

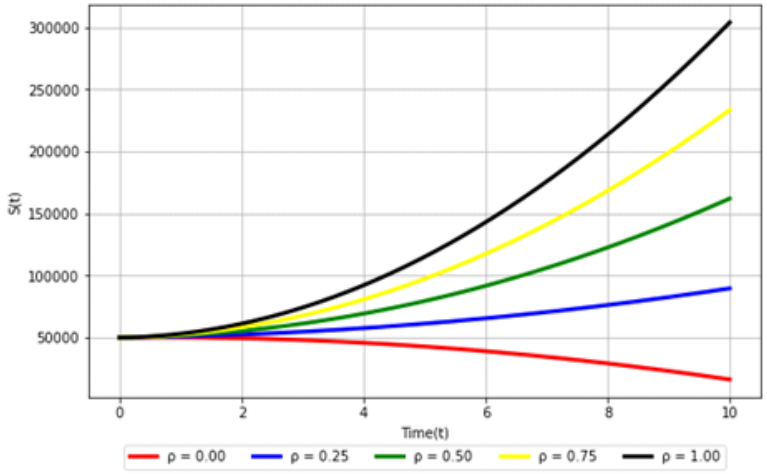

Figure 4. Influence of relapse rate of recovered individuals ρ on susceptible population

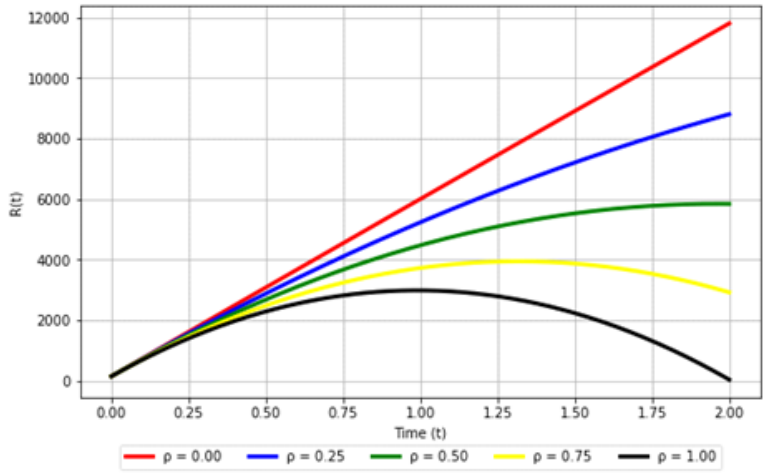

Figure 5. Influence of relapse rate of recovered individuals ρ on Recovered population

9. Discussion

Figure 2 shows how the number of susceptible individuals changes over a 10-month period, starting with an initial population of 50,000. Without any control measures in place (when $\alpha = 0$), the number of susceptible people actually increases, reaching a peak of about 70,000 within the first six months. This rise could be due to factors like population growth or people moving into the susceptible group. However, after this peak, the number begins to drop slightly, ending at around 65,000 by the 10^{th} month.

When control measures are introduced and gradually increased, the trend changes noticeably. With a 25% control rate ($\alpha = 0.25$), the susceptible population no longer grows as much and remains around 50,000 by the end of the period. This suggests that even moderate intervention can slow down the spread and keep more people from becoming susceptible.

As the level of control increases further, the number of susceptible individuals drops more sharply. At a 75% control rate, the population falls to about 18,000 by month 10. And when control is at its maximum100%the susceptible population drops to zero. This clearly shows that strong control measures are highly effective at reducing the number of people at risk of infection. Figure 3 illustrates how the recovered population, $R(t)$, changes over a 10-month period under different levels of control effectiveness. The graph starts with a small number of recovered individualsonly about 155. However, as time progresses, the number of recovered people grows significantly, with the final size depending heavily on the strength of the control measures in place.

When control is highly effective (100% control), the recovered population surpasses 70,000 by the end of the 10 months. This sharp increase suggests that with strong interventions (such as treatment, isolation, or vaccination), a large portion of the population successfully recovers from the infection.

In the case of a 75% control rate, the growth is still substantial but less dramatic, with the recovered population reaching around 50,000. On the other hand, when there is no control at all (0% effectiveness), the number of recovered individuals remains quite lowfewer than 10,000indicating limited recovery likely due to ongoing transmission and overwhelming spread of the disease.

Figure 4 explores how the susceptible population changes over 10 months depending on the rate at which recovered individuals relapse and return to the susceptible group (denoted by the parameter ρ).

With an initial value of 50,000, the susceptible population increases dramatically when the relapse rate is high. At a full relapse rate ($\rho = 1$), where all recovered individuals become susceptible again, the susceptible population grows to over 300,000 by the end of the 10-month period. This sharp rise indicates that continuous reinfection significantly fuels the pool of susceptible individuals.

As ρ decreases to 0.75, the increase in susceptibility slows, with the population reaching about 225,000. When the relapse rate is further reduced to 0.5 (i.e., only half of the recovered individuals become susceptible again), the susceptible population drops to below 170,000. This shows that reducing the likelihood of relapse significantly limits the size of the susceptible group and, by extension, the potential for new infections.

In the scenario where there is no relapse at all ($\rho = 0$), the susceptible population either remains constant or declines slightly over time due to other natural dynamics in the model. This suggests that preventing relapse plays a crucial role in maintaining control over disease spread.

Figure 5 illustrates how the recovery population evolves over time under different values of the relapse rate ρ, which represents the proportion of recovered individuals who lose immunity and return to the susceptible class.

The simulation begins with an initial recovery population of just 155. When the relapse rate is at its maximum ($\rho = 1$), the recovery population grows quickly, peaking at around 3,000, but then begins to decline within the 10-month period. This drop reflects the constant movement of individuals out of the recovered class and back into susceptibility.

As the relapse rate is reduced to $\rho = 0.75$, the recovery population reaches a higher peak of about 4,000 before declining to around 3,000. When the relapse rate drops further to $\rho = 0.5$, the number of recovered individuals rises more steadily, reaching approximately 6,000suggesting that fewer individuals are leaving the recovered class, allowing the group to grow.

In the scenario where there is no relapse at all ($\rho = 0$), the recovery population continues to rise throughout the 10-month period. This sustained increase is due to the continuous recruitment of individuals from other compartments (such as the infected class) into the recovered class, without any loss back to susceptibility.

10. Conclusion

The study demonstrates that the vaccination control rate, represented by α, significantly influences the dynamics of COVID-19 vaccination on disease susceptibility and recovery within a population. The findings reveal an inverse relationship between the vaccination control rate and the number of susceptible individuals, implying that higher vaccination coverage with a controlled α reduces the population's vulnerability to infection. Moreover, effective vaccination strategies contribute to an increase in the number of recovered individuals, highlighting the potential of vaccination to enhance overall immunity and expedite the recovery process.

However, the study also points to the challenge of relapse among recovered individuals, which can diminish immunity over time and potentially lead to increased susceptibility. Therefore, addressing waning immunity is crucial. Future research should focus on integrating booster vaccination campaigns and investigating the long-term efficacy of vaccines in mitigating relapse risks. These efforts could improve control of disease outbreaks and help sustain low transmission rates.

References

1. The pseudospectral Legendre method for solving the HIV infection model of CD4+ T cells. *Nonlinear Studies*, 25(1), 2018.
2. T. Abassy, E. Ahmed, S. El-Sayed, et al. Homotopy perturbation transform method for solving time-fractional order partial differential equations. *Ain Shams Engineering Journal*, 11:373–382, 2020.
3. J. Adedeji and M. O. Olayiwola. On analysis of a mathematical model of cholera using Caputo fractional order. *Journal of the Nigerian Mathematical Society*, 43(3):287–309, 2024.
4. I. Ahmed, G. Modu, A. Yusuf, P. Kumam, and I. Yusuf. A mathematical model of Coronavirus Disease (COVID-19) containing asymptomatic and symptomatic classes. *Results in Physics*, 21:103776, 2021.
5. T. Alade, M. Alnegga, S. Olaniyi, and A. Abidemi. Mathematical modelling of within-host chikungunya virus dynamics with adaptive immunity. *Modeling Earth Systems and Environment*, 2023.
6. A. Alaje and M. Olayiwola. A fractional-order mathematical model for examining the spatiotemporal spread of COVID-19 in the presence of vaccine distribution. *Healthcare Analytics*, 4, 2023.
7. A. Alaje, M. Olayiwola, K. Adedokun, and et al. Modified homotopy perturbation method and its application to analytical solitons of fractional-order Kortewegde Vries equation. *Beni-Suef University Journal of Basic and Applied Sciences*, 11:1–17, 2023.
8. A. Alaje, M. Olayiwola, M. Ogunniran, J. Adedeji, and K. Adedokun. Approximate analytical methods for the solution of fractional order integro-differential equations. *Nigerian Journal of Mathematics and Applications*, 31:175–190, 2021.
9. M. Aniji, N. Kavitha, and S. Balamuralitharan. Mathematical modelling of hepatitis B virus infection for antiviral therapy using LHAM. *Advances in Differential Equations*, 2020.
10. O. O. Asimiyu, A. O. Yunus, M. A. Omoloye, and M. O. Olayiwola. Novel approaches to malaria control and eradication using fractional-order modeling and numerical simulations. *Next Research*, page 100205, 2025.
11. T. A. Ayoola, M. K. Kolawole, and A. O. Popoola. Effects of acceptance of enlightenment on COVID-19 transmission using homotopy perturbation method. *Jambura Journal of Biomathematics (JJBM)*, 3(2):39–48, 2022.
12. T. A. Ayoola, M. K. Kolawole, and A. O. Popoola. Mathematical model of COVID-19 transmission dynamics with double dose vaccination. *Tanzania Journal of Science*, 48(2):499–512, 2022.
13. S. Balamuralitharan and S. Geethamalini. Solutions of epidemic of EIAV infection by HPM. In *Journal of Physics: Conference Series*, volume 1000, page 012023, 2018.
14. C. for Disease Control and Prevention. Chikungunya, 2023. Accessed: 10th March, 2023.
15. J. He. Homotopy perturbation technique. *Computational Methods in Applied Mechanics and Engineering*, 178(3-4):257, 1999.
16. J. He. Homotopy perturbation method for solving nonlinear equations. *Nonlinear Science Letters A*, 3(1):6–12, 2002.
17. J. He. Homotopy perturbation method: A new nonlinear analytical technique. *Applied Mathematics and Computation*, 135(1):73–79, 2003.
18. M. Kolawole, M. Olayiwola, A. Alaje, H. Adekunle, and O. K.A. Conceptual analysis of the combined effects of vaccination, therapeutic actions, and human subjection to physical constraint in reducing the prevalence of COVID-19 using the homotopy perturbation method. *Beni-Suef University Journal of Basic and Applied Sciences*, 12, 2023.
19. J. Koo, A. Cook, M. Park, et al. Interventions to mitigate Singapore's COVID-19 outbreak. *Nature*, 584:215–219, 2020.
20. F. Ndarou, M. Ngangue, and A. Akinwande. Modeling the COVID-19 outbreak in Wuhan, China: A mathematical approach. *Mathematical Modelling of Natural Phenomena*, 16(1):1–16, 2021.
21. M. Olayiwola and K. Adedokun. A novel tuberculosis model incorporating a Caputo fractional derivative and treatment effect via the homotopy perturbation method. *Bulletin of the National Research Centre*, 47(1):121, 2023.
22. M. Olayiwola, A. Alaje, A. Olarewaju, and K. Adedokun. A Caputo fractional order epidemic model for evaluating the effectiveness of high-risk quarantine and vaccination strategies on the spread of COVID-19. *Healthcare Analytics*, 3, 2023.
23. M. O. Olayiwola and K. A. Adedokun. A novel tuberculosis model incorporating a Caputo fractional derivative and treatment effect via the homotopy perturbation method. *Bulletin of the National Research Centre*, 47:121, 2023.
24. M. O. Olayiwola, A. I. Alaje, and A. O. Yunus. A Caputo fractional order financial mathematical model analyzing the impact of an adaptive minimum interest rate and maximum investment demand. *Results in Control and Optimization*, 14:100349, 2024.
25. T. Oreyeni, N. A. Shah, A. O. Popoola, E. R. Elzahar, and S. J. Yook. The significance of exponential space-based heat generation and variable thermophysical properties on the dynamics of Casson fluid over a stratified surface with non-uniform thickness. *Waves in Random and Complex Media*, pages 1–19, 2022.
26. K. Parand, Z. Kalantari, and M. Delkhosh. Quasilinearization-Lagrangian method to solve the HIV infection model of CD4 T cells. *SeMA*, 75:271–283, 2018.
27. K. Parand, H. Yousefi, M. Fotouhifar, M. Delkhosh, and M. Hosseinzadeh. Shifted Boubaker Lagrangian approach for solving biological systems. *International Journal of Bifurcation and Chaos*, 2018.
28. A. O. Popoola, I. G. Baoku, and B. I. Olajuwon. Heat and mass transfer on MHD viscoelastic fluid flow in the presence of thermal diffusion and chemical reaction. *International Journal of Heat and Technology*, 34(1):15–26, 2016.
29. A. O. Popoola, M. K. Kolawole, and M. O. Olayiwola. The effect of thin flame velocity and other sensitive factors on the maximum temperature of thermal explosion in the Earth's interior. *Journal of Science and Arts*, 17(3):573–580, 2017.
30. N. A. Shah, A. O. Popoola, T. Oreyeni, E. Omokhuale, and M. M. Altine. A modelling of bioconvective flow existing with tiny particles and quartic autocatalysis reaction across stratified upper horizontal surface of a paraboloid of revolution. *Mathematical Modelling and Numerical Simulation with Applications*, 3(1):74–100, 2023.
31. A. Yunus, M. Olayiwola, M. Omoloye, and A. Oladapo. A fractional-order model of Lassa disease using the Laplace-Adomian Decomposition Method. *Healthcare Analytics*, 3:100167, 2023.
32. A. O. Yunus and M. O. Olayiwola. Mathematical modeling of malaria epidemic dynamics with enlightenment and therapy intervention using the Laplace-Adomian decomposition method and Caputo fractional order. *Franklin Open*, page 100147, 2024.
33. A. O. Yunus and M. O. Olayiwola. The analysis of a novel COVID-19 model with the fractional-order incorporating the impact of the vaccination campaign in Nigeria via the Laplace-Adomian decomposition method. *Journal of the Nigerian Society of Physical Sciences*, pages 1830–1830, 2024.

